CHINESE OPTICS LETTERS
Vol. 22, No. 1 | January 2024

Long-term ultrastable frequency dissemination via a 50-km spooled fiber link using a two-section DFB laser

Zhiqian Yin (尹知谦)[1], Chuanbo Zhang (张川博)[1], Shijian Guan (管世健)[1], Xin Zhou (周 昕)[1], Yaguang Wang (王亚光)[1], Leilei Wang (王磊磊)[1], Manhang Zheng (郑满航)[1], Yitong Liu (刘奕彤)[1], Yunshan Zhang (张云山)[2], Xingbang Zhu (朱兴邦)[3], Tao Fang (方 涛)[1*], and Xiangfei Chen (陈向飞)[1**]

[1] Engineering Research Center of Precision Photonics Integration and System Application, Ministry of Education & Key Laboratory of Intelligent Optical Sensing and Manipulation, Ministry of Education & National Laboratory of Solid State Microstructures & College of Engineering and Applied Sciences & Institute of Optical Communication Engineering & Nanjing University-Tongding Joint Lab for Large-Scale Photonic Integrated Circuits, Nanjing University, Nanjing 210023, China

[2] College of Electronics and Optical Engineering and College of Flexible Electronics, Nanjing University of Posts and Telecommunications, Nanjing 210023, China

[3] The 41st Research Institute of China Electronics Technology Group Corp, Qingdao 266000, China

*Corresponding author: fangt@nju.edu.cn

**Corresponding author: chenxf@nju.edu.cn

Received August 26, 2023 | Accepted September 6, 2023 | Posted Online January 18, 2024

The stable long-distance transmission of radio-frequency (RF) signals holds significant importance from various aspects, including the comparison of optical frequency standards, remote monitoring and control, scientific research and experiments, and RF spectrum management. We demonstrate a scheme where an ultrastable frequency signal was transmitted over a 50 km coiled fiber. The optical RF signal is generated using a two-section distributed feedback (DFB) laser for direct modulation based on the reconstruction equivalent chirp (REC) technique. The 3-dB modulation bandwidth of the two-section DFB laser is 18 GHz and the residual phase noise of -122.87 dBc/Hz is achieved at 10-Hz offset frequency. We report a short-term stability of 1.62×10^{-14} at an average time of 1 s and a long-term stability of 6.55×10^{-18} at the measurement time of 62,000 s when applying current to the front section of the DFB laser. By applying power to both sections, the stability of the system improves to 4.42×10^{-18} within a testing period of 56,737 s. Despite applying temperature variations to the transmission link, long-term stability of 8.63×10^{-18} at 23.9 h can still be achieved.

Keywords: frequency dissemination; two-section DFB laser; phase stability.
DOI: 10.3788/COL202422.013903

1. Introduction

Radio-frequency (RF) signals play a crucial role in modern communication, radar, radio astronomy, and other fields. With the increasing demand for high precision and stability in communication systems and scientific instruments, stable transmission and accurate phase reference have become key challenges. Traditional RF signal transmission often relies on transmission media and cables, but it is constrained by issues such as electromagnetic interference, transmission loss, and phase drift, which limit the performance improvement of the system[1–6]. To address these challenges, fiber-optic-based RF phase-stable transmission technology has received extensive research and application in recent years. Fiber optics, as a low-loss and low-attenuation transmission medium, offers advantages such as high bandwidth, low transmission loss, and immunity to electromagnetic interference, making it an ideal choice for achieving high-precision and high-stability RF signal transmission[7–10]. Fiber transmission enables the conversion of RF signals to optical signals through electro-optic modulation and modulation–demodulation techniques, which are then transmitted and restored to RF signals through photoelectric conversion at the receiving end. Direct modulation lasers (DMLs) offer high modulation bandwidth, enabling high-speed data transmission to meet the demands of large-scale data transfer[11,12]. Additionally, DMLs achieve real-time performance and low latency, making them suitable for applications requiring quick response and real-time performance. Furthermore, this technology simplifies system architecture by replacing expensive modulators, reducing costs and complexity, while typically consuming less power, thus saving energy[13–15]. The use of the REC technique eliminates the need for electron-beam lithography in the fabrication of laser chips, resulting in lower manufacturing costs for analog DMLs[16–18]. The key factors for assessing the performance of phase-stable transmission include transmission distance, transmission signal frequency range, stability loss, testing time, temperature disturbance resilience, phase compensation range, system cost, and integration level, among others[19–22]. Currently, there are few systems in the research of long-distance frequency synchronization transmission that simultaneously meet all of these criteria.

In this paper, we propose a system design utilizing a two-section analog DML fabricated using the REC technique as the optical carrier RF transmission module for transmitting RF signals over a 50-km spooled fiber link. We present the characterization of the current-power curves and 3-dB modulation bandwidth of the analog DML and provide details on the experimental setup, techniques, and testing methods employed to achieve phase stability. We evaluate the long-term and short-term stability of the system whether DML applies current to the reflection section or not and investigate its resilience to temperature disturbances by introducing temperature variations in the transmission link.

2. Experimental Design

The schematic diagram of the phase-stable transmission system is shown in Fig. 1. The principle of phase stabilization in the entire transmission system is to actively detect the phase noise introduced during the link transmission at the central site and perform precompensation so that the remote-site users can use frequency signals consistent with the phase of a rubidium atomic clock. To measure the stability loss of the system transmission, both the central site and the remote site of the phase-stabilized transmission system are located within the Engineering Research Center of Precision Photonics Integration and System Application (Nanjing University), Ministry of Education. The transmission link uses a spooled 50 km G.652 optical fiber; such a setup makes the transmission link more sensitive to temperature changes and environmental vibrations. A portion of the optical signal transmitted to the remote site is demodulated

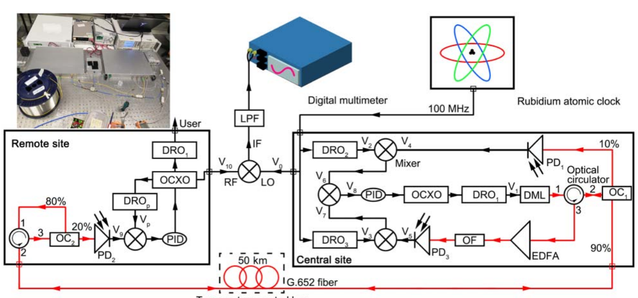

Fig. 1. Schematic of the phase-stable transmission system; the inset is an integrated phase-stable transmission system and the actual layout of the link. DRO, dielectric-resonant oscillator; OCXO, oven-controlled crystal oscillator; PID, proportional-integral-differential; OC, optical coupler; PD, photodetector; EDFA, erbium-doped fiber amplifier; OF, optical filter; LPF, low-pass filter.

by a photodetector (PD) to measure stability loss, while another portion carrying error signals is fed back to the central site via an optical circulator for compensation generation. The phase-stabilized transmission system compensates for the delay in the link by controlling the phase of an oven-controlled crystal oscillator (OCXO) using a proportional-integral-differential (PID) algorithm. The frequency signal generated by dielectric-resonant oscillator (DRO_1) is referred to as

$$V_1 = A\cos(\omega_1 t + \tau_1). \tag{1}$$

ω_1 is in the X-band. Due to variations in the signal amplitude caused by device performance, the signal amplitude will be disregarded in the subsequent equations. To measure the stability loss of the transmission system, it is necessary to determine the phase fluctuations caused by environmental effects during signal transmission in the optical fiber. Three DROs locked to a rubidium atomic clock are required to generate auxiliary signals, and the frequency signals generated by them are denoted as

$$\begin{aligned} V_2 &= \cos(\omega_2 t + \tau_2), \\ V_3 &= \cos(\omega_3 t + \tau_3), \\ V_p &= \cos(\omega_p t + \tau_p), \end{aligned} \tag{2}$$

and satisfy

$$\begin{cases} \omega_2 + \omega_3 = 2\omega_p \\ \tau_2 + \tau_3 = 2(\tau_p + \varepsilon) \end{cases}. \tag{3}$$

The V_1 signal generated by DRO_1 is modulated by the two-section analog DML and then passes through the optical circulator (OC) and OC_1 (20:80) before entering the fiber link. To further improve the stability of the transmission system, the environmental effects on the distance between the analog DML and OC_1 need to be taken into account. Twenty percent of the optical signal coupled out by OC_1 is collected by PD_1 and demodulated, resulting in an electrical signal,

$$V_4 = \cos(\omega_1 t + \tau_4), \tag{4}$$

where τ_4 carries the error information for this section. Most of the received optical signal at the remote site is sent back through the same path, except for a small portion that is demodulated by PD_2. The returned optical signal is amplified by the erbium-doped fiber amplifier (EDFA) and then passes through an optical filter (OF) to remove excess background noise before being detected and demodulated by PD_3. This results in an electrical signal,

$$V_5 = \cos(\omega_1 t + \tau_4 + 2\tau'), \tag{5}$$

where τ' represents the delay introduced by a single transmission on the link. By mixing V_2 and V_4, the difference frequency signal is obtained,

$$V_6 = \cos[(\omega_1 - \omega_2)t + (\tau_4 - \tau_2)], \tag{6}$$

and by mixing V_3 and V_5, the difference frequency signal is

$$V_7 = \cos[(\omega_3 - \omega_1)t + (\tau_3 - \tau_4 - 2\tau')]. \tag{7}$$

Finally, the difference frequency signal is obtained by mixing V_6 and V_7.

$$\begin{aligned} V_8 &= \cos[(2\omega_1 - \omega_2 - \omega_3)t + 2\tau_4 + 2\tau' - \tau_2 - \tau_3] \\ &= \cos[2(\omega_1 - \omega_p) + 2(\tau_4 + \tau' - \tau_p - \varepsilon)], \end{aligned} \tag{8}$$

where V_8 is the error signal applied to the OCXO. Since ε represents a fixed phase difference that does not affect the final frequency stability, it can be ignored. By continuously correcting the frequency and phase of the OCXO using V_8, it can satisfy

$$\begin{cases} \omega_1 = \omega_p \\ \tau_4 + \tau' = \tau_p \end{cases}. \tag{9}$$

Therefore, the signal V_6 demodulated by PD_2 at the far end can be expressed as

$$V_9 = \cos(\omega_1 t + \tau_4 + \tau') = \cos(\omega_p t + \tau_p), \tag{10}$$

which indicates that the phase of the demodulated signal V_9 at the remote site is locked to the frequency signal V_p at the central site, achieving stable frequency transmission and synchronization.

3. Results and Discussion

The DML plays a crucial role in phase-stable transmission systems. As an optical carrier RF transmission module, it is responsible for modulating the desired RF signal onto the optical carrier. By modulating the laser's current directly, RF signals can be transmitted over the fiber link without the need for an external modulator. The stability and performance of the DML directly impact the quality and reliability of the phase-stable transmission system.

In light of this, we have developed an analog DML that meets the requirements for high-precision phase-stable transmission. The schematic diagram of the two-section analog DML chip is shown in Fig. 2(a). The designed laser chip consists of a laser section (LS) and a reflection section (RS). The design of the LS is similar to a standard DFB laser, with a $\lambda/4$ shift added in the center of the grating layer. Antireflection (AR) coatings are applied to both surfaces to ensure wavelength accuracy. The wavelength of the laser is mainly determined by the sampling period in the laser section. The cavity length of the LS is 400 μm. Since power loss in optical signal transmission over long distances is inevitable, it is necessary for the laser to have a sufficiently high initial output power to overcome the degradation of the signal-to-noise ratio with increasing transmission distance. Therefore, the cavity length is designed to be relatively long. Considering the duty cycle of the sampled grating, the effective coupling coefficient is approximately $3000\,\mathrm{m}^{-1}$. Due to the

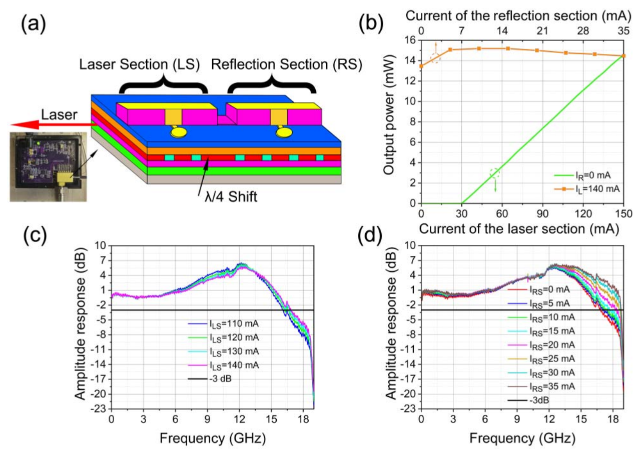

Fig. 2. (a) Schematic of two-section analog DML; the inset is a picture of the analog DML chip after packaging and in use. (b) *P-I* curves of the two-section analog DML; (c) modulation amplitude response of the two-section analog DML when I_{RS} = 0 mA; (d) modulation amplitude response of the two-section analog DML when I_{LS} = 140 mA.

presence of strong feedback in the RS, it is required to have a slightly smaller normalized coupling coefficient in the LS (less than 1.2) to ensure stable single-mode characteristics. The cavity length of the RS is 600 μm, and there is no phase shift in the grating layer. The LS and RS share a common seed grating, and the effective coupling coefficient of the reflection section is also $3000\,\mathrm{m}^{-1}$, which greatly reduces the fabrication requirements. Additionally, both the LS and RS have a duty cycle of 0.5, maximizing the coupling strength of the grating. The two-section analog DML fabricated using the REC technology not only has low production costs but also offers high wavelength accuracy.

The inset shows the packaged form of the analog DML chip. Static characteristics testing was performed on the packaged analog DML. Figure 2(b) shows the power-bias current *(P-I)* curves of the two-section analog DML. The green line represents the output power of the laser when the current of the RS is 0 mA and the current of the LS varies. The orange line represents the output power of the laser when the current of the LS is 140 mA and the current of the RS varies. The threshold current of the two-section analog DML is 30 mA, which can be optimized by increasing the grating coupling coefficient. Due to the longer cavity length designed, the two-section analog DML exhibits a higher saturated output power. Even when the current reaches 150 mA, the laser output power is still not saturated. Due to absorption loss, the feedback effect from the RS is weak when $I_{RS} = 0$ mA. When a small current is injected into the RS, the feedback is enhanced, leading to a significant increase in the laser output power. As the injected current into the RS continues to increase, the output power of the two-section analog DML reaches saturation. Figures 2(c) and 2(d) present the measurement results of the modulation bandwidth of the two-section analog DML using a vector network analyzer. When no current is injected into the RS, the analog DML behaves similarly to an unadventurous DFB laser with AR–AR coatings. As the injected current into the LS increases (I_{LS} = 110, 120, 130, 140 mA), the modulation bandwidth of the analog DML also increases. When I_{LS} = 150 mA, the modulation bandwidth reaches its maximum value, approximately 16 GHz. With the continuous increase in the injected current into the RS (I_{RS} = 0, 5, 10, 15, 20, 25, 30, 35 mA), the modulation bandwidth of the analog DML further increases and can reach 18 GHz. This bandwidth is also covering the entire X-band.

To estimate the performance of the phase-stable transmission system, it is necessary to compare the received frequency signal V_{10} at the remote site with the reference frequency signal V_0 in terms of relative phase. This provides the frequency stability of V_{10} relative to V_0, representing the overall transmission stability of the system. Currently, the industry-standard frequency measurement instruments are the Microsemi 5125A from the United States and the VCH 320 from Russia. Due to limitations in measurement techniques (dual-mixing measurement) of these instruments, their long-term stability is difficult to measure at the level of 10^{-18}. Under special measurement conditions (e.g., constant temperature, ultra-quiet environment, seismic resistance), they can achieve a stability level of 10^{-18}.

Therefore, the dedicated frequency stability measurement instrument, Microsemi 5125A, does not meet the measurement requirements. Instead, a direct mixing method is proposed to directly evaluate the RF transmission performance. The principle is to mix the recovered RF signal V_{10} at the terminal station with the source signal V_0. Since the frequencies of the two input signals are the same, the relative phase variation between the two input signals can be reflected by the amplitude fluctuation of the mixer output voltage. By using a high-precision voltmeter (Keithley 2010) to measure the voltage $V(t)$ at the intermediate frequency (IF) port of the mixer, the corresponding relative delay fluctuation $\Delta\varphi(t)$ can be deduced. This can be used for calculating the frequency stability. In Fig. 1, the local oscillator (LO) input of the mixer serves as the reference frequency source,

$$V_0 = A\cos\omega t. \tag{11}$$

The RF input of the mixer is the signal to be phase-detected,

$$V_{10} = B\cos[\omega t + \Delta\varphi(t)]. \tag{12}$$

The difference frequency signal obtained after mixing V_0 and V_{10}, which have the same frequency but a phase difference $\Delta\varphi(t)$, is

$$V_{IF}(t) = C\cos\Delta\varphi(t) + D, \tag{13}$$

where C represents the amplitude of the beat frequency signal, and D is the output DC potential. The measurement value of V_{IF} can be monitored in real time using a digital multimeter. By manually changing the phase of the RF input signal to allow $\Delta\varphi(t)$ to undergo a phase change of 2π, the maximum value V_{IFmax} and minimum value V_{IFmin} will appear when $\Delta\varphi(t)$ takes the values of 0 and π, respectively. Through simple calculations, C and D can be expressed using the known maximum and minimum values,

$$\begin{cases} C = \frac{V_{IFmax} - V_{IFmin}}{2} \\ D = \frac{V_{IFmax} + V_{IFmin}}{2} \end{cases}. \tag{14}$$

Thus, the phase difference can be inferred from the measured values of V_{IF} as

$$\Delta\varphi(t) = \arccos\left[\frac{2V_{IF}(t) - (V_{IFmax} + V_{IFmin})}{V_{IFmax} - V_{IFmin}}\right]. \tag{15}$$

The corresponding relative time delay fluctuation, $\Delta\Phi(t)$, is given by

$$\Delta\Phi(t) = \frac{\Delta\varphi(t)}{2\pi\omega} = \frac{\arccos\left[\frac{2V_{IF}(t) - (V_{IFmax} + V_{IFmin})}{V_{IFmax} - V_{IFmin}}\right]}{2\pi\omega}. \tag{16}$$

Once the value of $\Delta\Phi(t)$ is obtained, it can be used for calculating the frequency stability. The 50 km fiber spool is placed in the temperature control box shown in Fig. 1, and the temperature is varied dramatically to allow $\Delta\varphi(t)$ to change over a complete cycle, resulting in obtaining V_{IFmax} and V_{IFmin}. Figure 3(a) shows the variation of V_{IF} measured by the digital multimeter within a period of 62,000 s. It can be observed that the voltage changes only by 0.179 mV during the measurement period. Figure 3(b) represents the inferred phase fluctuation based on the V_{IF} variation. The black line represents the compensated link delay jitter, while the red line represents the jitter of the system in free transmission. From the graph, it can be seen that the link delay variation of the fiber link in the free transmission is approximately 600 ps, whereas in the compensated system, the transmission time delay of the signal changes by only about 1.15 ps during the testing time.

Phase noise of the frequency signal is an important indicator for measuring short-term frequency stability. We measured the phase noise of the rubidium atomic clock reference signal (100 MHz) and the compensated/uncompensated frequency signal (100 MHz) after a 50 km transmission using a signal and spectrum analyzer. The results are shown in Fig. 4(a). The difference between the red and black lines can be used to evaluate the degradation of phase noise caused by environmental influences during fiber link transmission. It is mainly distributed

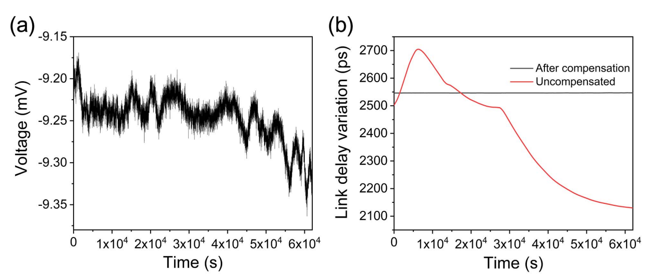

Fig. 3. (a) Measured V_{IF} in the phase-stable transmission system; (b) 50 km fiber link delay variation before and after compensation.

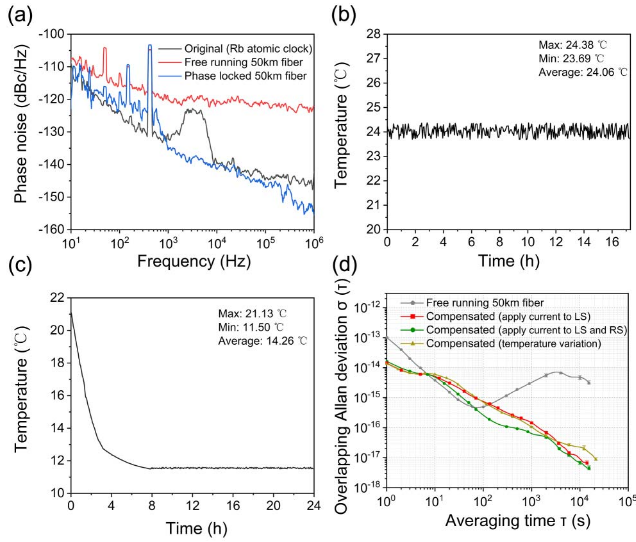

Fig. 4. (a) Phase noise of the frequency signal through 50 km fiber link (black, original Rb atomic clock; red, free running; blue, phase-locked). Temperature monitoring of the temperature control box. (b) Constant temperature; (c) variable temperature; (d) fractional frequency instability of the 50 km free-running link (gray pentagons); compensated link at 100 MHz when applying current to RS or not (green circles/red squares), and compensated link during temperature fluctuations (golden triangles) versus averaging time.

across the entire frequency offset range, indicating a significant deterioration of phase noise in long links. When the transmitted frequency signal is compensated, the phase noise is greatly reduced. At a 10 Hz offset from the carrier, the measured phase noise is -122 dBc/Hz. Near the hundred-hertz range, there is a noticeable peak observed, which is caused by the bandwidth of the control loop.

To test the temperature disturbance resistance of the phase-locked transmission system, a 50 km fiber spool was placed in a temperature control box to create an artificial temperature variation. First, temperature sensors were used to record the temperature of the fiber optic at room temperature, with an average temperature of 24.06°C and fluctuations of about 0.69°C, as shown in Fig. 4(b). Then, the temperature of the fiber environment was lowered from 21.13°C to 11.50°C, with a decrease of 9.63°C in about 8 h; it stabilized around 11.5°C, as shown in Fig. 4(c). This temperature variation is more severe than what the fiber would experience in actual deployment, as in real installations, the fiber length is longer and buried underground, resulting in less drastic temperature changes in terms of range and rate. As shown in Fig. 4(d), the frequency stability of the 50 km fiber transmission system was measured using the direct mixing method. To achieve better testing results, fiber-matching gel was applied to both ends of the fiber connectors. When only the LS of the analog DML is powered, it can be observed that the frequency stability of the system was significantly improved by nearly 3 orders of magnitude, reaching 6.55×10^{-18} at an average measurement time of 62,000s. When both the LS and RS of the analog DML are powered, the frequency stability is further optimized, reaching 4.42×10^{-18} after a measurement time of 56,737 s. This is because the designed analog DML, when powered at the LS and RS, reduces the DML linewidth. Narrower linewidth results in higher frequency stability, lower noise, and increased coherence, thereby improving the performance of the phase-stable transmission system. Based on the measured time delay fluctuation $\Phi(t)$ during the stability testing process, the average value μ was calculated using the following formula:

$$\sigma = \sqrt{\frac{\sum_{i=1}^{n} (\Phi_i - \mu)^2}{n}}. \tag{17}$$

By substituting the measured samples of $\Phi(t)$ into the formula, the frequency stability accuracy of the transmission system can be calculated. The calculated stability accuracy of the system is 0.04 ps. Although there is a slight decrease in frequency stability due to temperature-induced noise, it still reaches the level of 10^{-18}, indicating that the system is capable of mitigating delay fluctuations caused by temperature variations within the corresponding range, using the formula

$$\delta = KLT. \tag{18}$$

The delay fluctuations caused by temperature disturbances in the fiber link can be measured in a phase-stable transmission system. Given the average temperature coefficient of the fiber, K, as 35.1 ps/(km °C), the transmission link distance, L, as 50 km, and the temperature variation range, T, as 9.63°C, the value of δ is calculated to be 17.55 ns, which represents the phase compensation range of the stable transmission system as tens of nanoseconds. More importantly, after a 10 s latency, the stability $\sigma(\tau)$ of the transmission system is inversely proportional to the running time $1/\tau$, showing a typical stability curve of a phase-locked loop. The short-term stability of the transmission system is not significantly affected by the inclusion of temperature variations, remaining at the level of 10^{-14}, indicating that temperature variations mainly affect long-term stability.

4. Conclusions

In this paper, we proposed a two-section analog DML based on REC technology, which achieves an output power exceeding 14 mW and a modulation bandwidth of up to 18 GHz. We applied this laser to a phase-stable transmission system. The experimental results demonstrate that the RF signal in the X-band, after being transmitted through a 50 km fiber link, exhibits a stability of 1.62×10^{-14} at 1 s and a stability of 9.17×10^{-18} at 10^4 s for a 100 MHz RF signal when the RS is not powered. When the RS is powered, the stability can be optimized to 6.96×10^{-18} at 10^4 s. Even with a temperature variation of approximately 10°C introduced to the transmission link within 8 h, the fiber transmission stability is still maintained within the range of 10^{-14} and 10^{-18}, with average times of 1 s and 86,050 s, respectively. This proves that the system has excellent resistance to temperature disturbances and a wide phase compensation range.

By optimizing the link structure, especially in overcoming backward Rayleigh scattering, and combined with REC technology to improve the slope efficiency of a DFB laser, further improvement in the transmission stability of frequency signals can be achieved. Efforts are under way to optimize the operation of the phase-stable transmission system; the results will be published in a separate paper.

Acknowledgements

This work was supported by the National Key R&D Program of China (No. 2020YFB2205804), the National Natural Science Foundation of China (Nos. 62273355, 61975075, 61975076, and 62004094), the Natural Science Foundation of Jiangsu Province of China (No. BK20200334), and the Jiangsu Science and Technology Project (No. BE2017003-2).

References

1. O. Lopez, F. Kéfélian, H. Jiang, *et al.*, "Frequency and time transfer for metrology and beyond using telecommunication network fibres," C. R. Phys. **16**, 531 (2015).
2. C. Q. Ma, L. F. Wu, Y. Y. Jiang, *et al.*, "Optical coherence transfer over 50-km spooled fiber with frequency instability of 2×10^{-17} at 1 s," Chin. Phys. B **24**, 084209 (2015).
3. Z. T. Feng, X. Zhang, R. Wu, *et al.*, "Coherent optical and RF receiver for simultaneously transferring frequencies in optical and RF domain," in *Joint Conference of the IEEE International Frequency Control Symposium and European Frequency and Time Forum* (2019), p. 1.
4. D. Hou, P. Li, P. Xi, *et al.*, "Timing jitter reduction over 20-km urban fiber by compensating harmonic phase difference of locked femtosecond comb," Chin. Opt. Lett. **8**, 993 (2010).
5. O. Lopez, A. Haboucha, F. Kéfélian, *et al.*, "Cascaded multiplexed optical link on a telecommunication network for frequency dissemination," Opt. Express **18**, 16849 (2010).
6. M. Musha, F. L. Hong, K. Nakagawa, *et al.*, "Coherent optical frequency transfer over 50-km physical distance using a 120-km-long installed telecom fiber network," Opt. Express **16**, 16459 (2008).
7. H. Kiuchi, "Highly stable millimeter-wave signal distribution with an optical round-trip phase stabilizer," IEEE Trans. Microw. Theory Tech. **56**, 1493 (2008).
8. X. Wang, W. Wei, Z. Liu, *et al.*, "Joint frequency and time transfer over optical fiber with high-precision delay variation measurement using a phase-locked loop," IEEE Photonics J. **11**, 5501208 (2019).
9. H. Jiang, F. Kéfélian, S. Crane, *et al.*, "Long-distance frequency transfer over an urban fiber link using optical phase stabilization," J. Opt. Soc. Am. B **25**, 2029 (2008).
10. D. Hou, P. Li, C. Liu, *et al.*, "Long-term stable frequency transfer over an urban fiber link using microwave phase stabilization," Opt. Express **19**, 506 (2011).
11. Y. Zhang, B. Yuan, L. Li, *et al.*, "Experimental demonstration of single sideband modulation utilizing monolithic integrated injection locked DFB laser," J. Lightwave Technol. **38**, 1809 (2020).
12. S. Guan, Y. Zhang, B. Yuan, *et al.*, "Research on the asymmetric corrugation-pitch-modulated HR-AR DFB lasers with sampled gratings," J. Lightwave Technol. **39**, 4725 (2021).
13. J. Wang, C. Yue, Y. Xi, *et al.*, "Fiber-optic joint time and frequency transfer with the same wavelength," Opt. Lett. **45**, 1 (2020).
14. Y. Cui, T. Jiang, S. Yu, *et al.*, "Passive-compensation-based stable RF phase dissemination for multiaccess trunk fiber link with anti-GVD and anti-backscattering function," IEEE Photonics J. **9**, 7203608 (2017).
15. Z. Li, L. Yan, Y. Peng, *et al.*, "Phase fluctuation cancellation of anonymous microwave signal transmission in passive systems," Opt. Express **4**, 16 (2014).
16. Z. Sun, Z. Su, R. Xiao, *et al.*, "Tunable laser via high-density integration of DFB lasers with high precision wavelength spacings," IEEE Photon. Technol. Lett. **34**, 467 (2022).
17. Y. Zhang, Y. Liu, J. Lu, *et al.*, "DFB laser arrays based on the REC technique and their applications in radio-over-fiber systems [Invited Paper]," Chin. Opt. Lett. **15**, 080603 (2017).
18. Z. Sun, Y. Wang, R. Xiao, *et al.*, "Directly modulated 25 Gbaud/s tunable in-series DFB laser array for WDM systems," Chin. Opt. Lett. **21**, 011403 (2023).
19. S. Foreman, K. Holman, D. Hudson, *et al.*, "Remote transfer of ultrastable frequency references via fiber networks," Rev. Sci. Instrum. **78**, 021101 (2007).
20. Z. Li, L. Yan, Y. Peng, *et al.*, "Enhanced phase stability in passive analog photonic links with coherent Rayleigh noise reduction," Opt. Express **23**, 5744 (2015).
21. M. Fujieda, M. Kumagai, T. Gotoh, *et al.*, "Ultrastable frequency dissemination via optical fiber at NICT," IEEE Trans. Instrum. Meas. **58**, 1223 (2009).
22. X. Wang, Z. Liu, S. Wang, *et al.*, "Photonic radio-frequency dissemination via optical fiber with high-phase stability," Opt. Lett. **40**, 2618 (2015).